

Angular momentum transport in protostellar discs

Raquel Salmeron¹, Arieh Königl¹ & Mark Wardle²

¹Department of Astronomy & Astrophysics, The University of Chicago, Chicago IL 60637, USA

²Physics Department, Macquarie University, Sydney NSW 2109, Australia

2006 November 6

ABSTRACT

Angular momentum transport in protostellar discs can take place either radially, through turbulence induced by the magnetorotational instability (MRI), or vertically, through the torque exerted by a large-scale magnetic field that threads the disc. Using semi-analytic and numerical results, we construct a model of steady-state discs that includes vertical transport by a centrifugally driven wind as well as MRI-induced turbulence. We present approximate criteria for the occurrence of either one of these mechanisms in an ambipolar diffusion-dominated disc. We derive “strong field” solutions in which the angular momentum transport is purely vertical and “weak field” solutions that are the stratified-disc analogues of the previously studied MRI channel modes; the latter are transformed into accretion solutions with predominantly radial angular-momentum transport when we implement a turbulent-stress prescription based on published results of numerical simulations. We also analyze “intermediate field strength” solutions in which both modes of transport operate at the same radial location; we conclude, however, that significant spatial overlap of these two mechanisms is unlikely to occur in practice. To further advance this study, we have developed a general scheme that incorporates also the Hall and Ohm conductivity regimes in discs with a realistic ionization structure.

Key words: accretion, accretion discs – ISM: jets and outflows – MHD – stars: formation.

1 INTRODUCTION

The mechanisms responsible for transporting angular momentum in protostellar discs are still not well understood. Perhaps the most generally relevant processes are:

(a) Radial transport through turbulence induced by the magnetorotational instability (MRI; e.g. Balbus & Hawley 1998). The MRI acts, essentially, by converting the free energy of differential rotation into turbulent motions that transfer angular momentum radially outward via the Maxwell stress of small-scale, disordered magnetic fields.

(b) Vertical transport by outflows driven centrifugally from the disc surfaces (e.g. Königl & Pudritz 2000). The transfer of angular momentum from the inflowing gas to the wind is mediated by a large-scale, ordered magnetic field that threads the disc (likely corresponding to interstellar field lines advected inward by the accretion flow but possibly generated locally by a disc dynamo).

Radial angular-momentum transport has been the hallmark of generic viscous disc models, for which the MRI process is thought to provide the most cogent physical basis. On the other hand, the ubiquity of bipolar outflows and jets in protostars and the apparent correlation between outflow and accretion signatures in these systems (e.g. Hartigan et al. 1995) have led to the suggestion that disc outflows might

be a key ingredient of the accretion process on account of the high angular-momentum transport efficiency of centrifugally driven winds (e.g. Königl 1989). The possibility of a central role for vertical angular-momentum transport is supported by recent *HST* observations of protostellar jets, which have been interpreted in terms of magnetocentrifugal winds carrying a large fraction of the excess angular momentum of the accreted matter from the inner regions ($r \lesssim 1$ AU) of the associated discs (see Ray et al. 2006 for a review). Although thermal pressure may contribute to the driving of the outflows (e.g. Pesenti et al. 2004), the stresses exerted by a large-scale magnetic field dominate the flow acceleration and collimation (Blandford & Payne 1982, hereafter BP82; see, however, Soker & Regev 2003 for an alternative view of the importance of thermal acceleration) and are the key to the efficient vertical angular-momentum transport indicated by the *HST* measurements.

Previous analytic and numerical investigations have considered the above two mechanisms under various simplifying assumptions. MRI studies have examined both the linear and nonlinear stages of the instability (e.g. Sano & Stone 2002a,b; Salmeron & Wardle 2003, 2005). The long-term global evolution of the instability in vertically stratified discs that are threaded by a single-polarity magnetic

field is still an open question (e.g. Miller & Stone 2000). The study of wind-driving discs has been complicated by the need to solve simultaneously for the inflow and outflow structures and by the non-local nature of the MHD solution. Progress has nevertheless been made semi-analytically by adopting a self-similarity formulation (e.g. Wardle & Königl 1993, hereafter WK93; Li 1995, 1996; Ferreira 1997) as well as numerically, with recent simulations reporting an evolution to a quasi-stationary state (e.g. Casse & Keppens 2002; Kuwabara et al. 2005). Since protostellar discs are weakly ionized over most of their extent, magnetic diffusivity effects have to be taken into account in modeling the accretion flow in both cases. In particular, both the MRI-driven turbulence and the centrifugal wind-launching mechanism require a minimum level of field-matter coupling to be effective (e.g. WK93; Sano & Inutsuka 2001). Therefore, the detailed ionization structure and conductivity properties of the disc need to be determined in order to incorporate either one of these processes into a realistic model.

Angular momentum removal from real discs is likely to involve both the radial and vertical transport mechanisms discussed above.¹ There have been a few attempts in the literature to construct quasi-steady disc models in which both of these mechanisms operate (e.g. Lovelace et al. 1994; Casse & Ferreira 2000; Ogilvie & Livio 2001), but these treatments invariably used a prescription for radial angular-momentum transport that did not explicitly account for its origin in MRI-induced turbulence. However, the fact that disc regions in which the entire excess angular momentum is carried away by a centrifugally driven wind are generally stable to the fastest growing mode of the MRI (WK93) indicates that a more refined approach is required. Broadly speaking, the MRI is suppressed in regions where the ratio $a \equiv v_{Az}/c_s$ of the Alfvén speed corresponding to the vertical field component B_z and the isothermal sound speed is comparatively large ($\gtrsim 1$); it may be expected to evolve into a fully developed turbulence when $a \ll 1$ (provided also that the gas is well coupled to the field). Since the value of a increases with distance z from the disc midplane, these considerations suggest that it could in principle be possible for both vertical and radial angular-momentum transport to take place at the same disc radius r , with the radial transport confined to a given range in z and with the vertical transport dominating at greater heights.

The purpose of this paper is to construct semi-analytic models of protostellar discs that incorporate both centrifugally driven winds and MRI-induced turbulence and to identify the relevant parameter regimes where either one of these two mechanisms dominates the angular momentum transport. We pay particular attention to the possibility that both of these mechanisms operate at the same disc radius and consider how they might affect each other in that case. We describe our wind-driving disc model (formulated following WK93) and present an illustrative solution of a disc with a predominantly vertical angular momentum transport

¹ Vertical angular momentum transport could alternatively take place through the process of magnetic braking, which involves the propagation of torsional Alfvén waves into the surrounding interstellar medium. This possibility is neglected in what follows, but see Krasnopol'sky & Königl (2002).

in Section 2. In Section 3 we outline our method of including MRI-induced turbulence (taking account of recent numerical simulations of the nonlinear evolution of the MRI) and illustrate it with a solution of a disc with a predominantly radial angular-momentum transport. We then consider the case of combined transport by wind and turbulence in Section 4 and summarize our results in Section 5.

2 VERTICAL TRANSPORT

We have devised a general scheme for modeling wind-driving protostellar discs using a tensor-conductivity formalism and a realistic vertical ionization structure.² The conductivity tensor makes it possible to include in a systematic way the three relevant magnetic diffusion mechanisms (ambipolar, Hall and Ohmic). The solutions presented in this paper are, however, derived under the simplifying assumptions of pure ambipolar diffusivity and (except in Section 4) constant ion density. This enables us to apply the analytic results obtained for this case in WK93 to the formulation of a prescription for MRI-induced turbulent transport in a wind-driving disc model. A wider class of solutions of our general scheme will be presented in future publications.

Our wind solutions are based on the magnetocentrifugal mechanism for “cold” disc outflows proposed by BP82. In this scenario, matter at the disc surface is accelerated by magnetic stresses if the open magnetic field lines that thread the disc are inclined at a sufficiently large angle to the rotation axis (the “bead-on-a-wire” effect), potentially reaching super-Alfvénic speeds. Our modeling procedure is based on that of WK93 and we refer the reader to that study for further details. In brief, we solve the mass and momentum conservation equations for the neutral gas, and the induction equation for the evolution of the magnetic field, assuming a steady-state, geometrically thin and nearly Keplerian accretion disc and neglecting all radial derivatives except that of v_ϕ . The disc is further assumed to be isothermal and weakly ionized. The latter condition implies that ionization and recombination processes, as well as the inertia and thermal pressure of the charged particles, have a negligible dynamical effect. In this limit, separate equations for the ionized species are not needed, and their effect on the neutrals can be conveyed by means of a conductivity tensor $\sigma(r, z)$ (assuming cylindrical polar coordinates; see Wardle 1999 and references therein). In addition, the field must satisfy $\nabla \cdot \mathbf{B} = 0$ (which in the thin-disc approximation implies that B_z can be assumed not to vary with height in the disc), whereas the current density \mathbf{J} must satisfy Ampère's and Ohm's laws.

The foregoing equations are integrated vertically from the midplane (indicated by a subscript 0) up to the position z_s of the critical (sonic) point, and the values of the physical variables there are estimated. The solution is then integrated

² The main ionization sources outside the innermost ~ 0.1 AU from the central object are nonthermal: interstellar cosmic rays, X-ray and UV radiation emitted by the magnetically active protostar and the decay of radioactive elements present in the disc. The gas near the disc surface is ionized primarily by X-rays in the vicinity of the star, and by UV photons (with a contribution also from the interstellar radiation field) in the outer disc (e.g. Semenov et al. 2004; Glassgold et al. 2005).

backward to a fitting point and iterated until full convergence is reached. The resulting disc solution is matched on to a global BP82-type self-similar wind solution, obtained by imposing the regularity condition at the Alfvén critical point. This final step effectively determines the value of B_ϕ at the disc surface (subscript b, defined as the height where v_ϕ equals the Keplerian speed v_K). The overall solution is determined by the following parameters:

(i) $a_0 = v_{Az,0}/c_s$, the midplane ratio of the Alfvén speed (based on the uniform vertical field component) to the sound speed, which measures the magnetic field strength.

(ii) η , the ratio of the Keplerian rotation time $\Omega_K^{-1} = r/v_K$ to the neutral-ion momentum-exchange time (see WK93); this parameter measures the degree of coupling between the neutrals and the ionized gas component (and magnetic field) and does not vary with height if the ion density is constant.³

(iii) $\epsilon \equiv -v_{r0}/c_s$, the normalized inward radial speed at the midplane. In practice, the value of this parameter is determined in our solutions (for given values of the other parameters) by imposing the Alfvén critical-point constraint on the wind.

(iv) $c_s/v_K = h_T/r$, the ratio of the tidal scale height to the radius – a measure of the geometric thinness of the disc.

(v) $\epsilon_B \equiv -cE_\phi/c_s B_z$, the normalized azimuthal component of the electric field \mathbf{E} . This parameter vanishes in a strictly steady-state solution but is nonzero if the magnetic field lines drift radially. Our formulation remains valid if the field-line drift speed is small compared to $|v_r|$ (see WK93).⁴

Fig. 1 shows an example of a local disc solution that matches on to a global BP82 wind solution. This solution resembles the one presented in Fig. 10 of WK93, although it was derived for a different choice of the parameters η and a_0 . Both of these solutions illustrate the main properties of wind-driving, strongly magnetized ($a_0 \lesssim 1$) discs. In the quasi-hydrostatic layer just above the midplane the magnetic field lines are (radially) bent and (azimuthally) sheared and the field removes angular momentum from the matter. The scale height h in this region is reduced by magnetic squeezing, which dominates the tidal compression. Above this layer lies a transition region where the magnetic energy comes to exceed the gas internal energy and the field lines are locally straight. In both of these zones, the fluid

³ In the more general formulation, one needs to specify the values of the independent components of the conductivity tensor – viz. the field-aligned (σ_{\parallel}), Pedersen (σ_P) and Hall (σ_H) conductivities. In this case, the magnetic coupling is expected to *decrease* with height in the ambipolar diffusion-dominated upper section of the disc, where the ion density is most strongly affected by the decrease of the neutral gas density with z (e.g. Salmeron & Wardle 2005). In the simplified approach adopted in this paper we use the parameter $\eta = (4\pi c_s^2/c^2)a^2(\sigma_P/\Omega_K)$ instead (with $a \propto \rho^{-1/2}$ increasing with z) and (except in Section 4) assume that it remains constant with height.

⁴ Our ansatz $\epsilon_B = 0$ effectively fixes the value of B_r at the disc surface. In a generalization to a global treatment, $B_{r,b}$ would be determined by the radial distribution of B_z along the disc (e.g. Ogilvie & Livio 2001; Krasnopolksy & Königl 2002), and the value of ϵ_B could be inferred from the overall magnetic field structure and the disc conductivity.

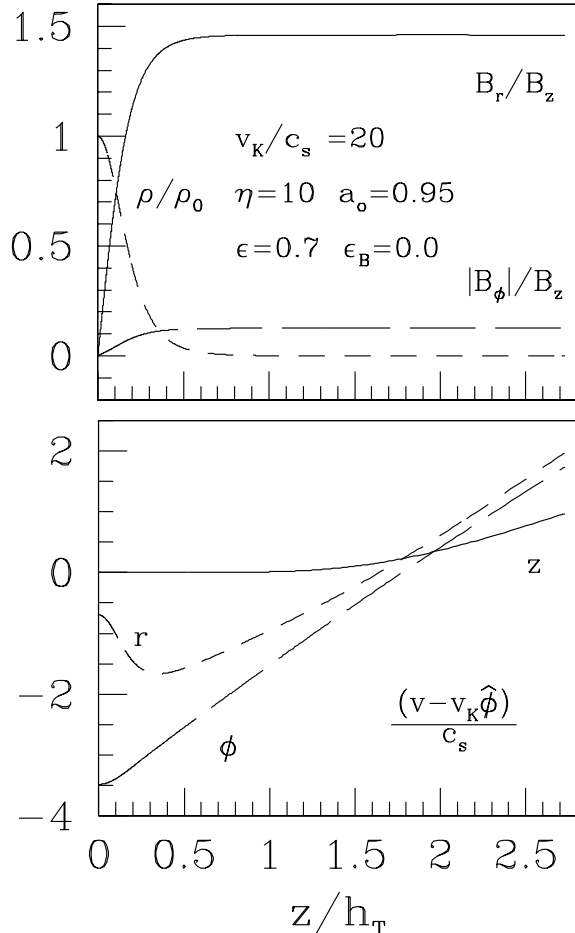


Figure 1. Vertical structure of a strongly magnetized, wind-driving disc. *Top:* B_r , $|B_\phi|$, and ρ . *Bottom:* velocity components. The curves terminate at the sonic point. The disc solution parameters are indicated in the figure. The corresponding parameters of the BP82 self-similar wind solution are $\kappa = 3.2 \times 10^{-4}$ (normalized mass-to-magnetic flux ratio), $\lambda = 395$ (normalized total specific angular momentum), and $\xi_b' \equiv B_{r,b}/B_z = 1.46$.

azimuthal speed is sub-Keplerian. Since the gas angular velocity decreases with radius, the field lines (which move with a constant angular velocity) eventually overtake the matter and fling it out centrifugally. The region where v_r and $(v_\phi - v_K)$ become positive constitutes the base of the wind. It has been shown (WK93; Königl 1997) that solutions of this type satisfy

$$(2\eta)^{-1/2} \lesssim a_0 \lesssim \sqrt{3} \lesssim \epsilon\eta \lesssim v_K/2c_s. \quad (1)$$

The first inequality in equation (1) expresses the requirement that the fluid remain sub-Keplerian below the wind-launching region, the second gives the wind launching condition ($B_{r,b}/B_z > 1/\sqrt{3}$), and the third gives the constraint that the base of the wind be located above a density scale height. The first two conditions imply a minimum value for the field-matter coupling parameter η (which a more detailed analysis sharpens to $\eta > 1$), whereas the last two imply that magnetic squeezing dominates the vertical confinement of the disc ($h < h_T$). The last inequality specifies that the rate of ambipolar diffusion heating at the midplane

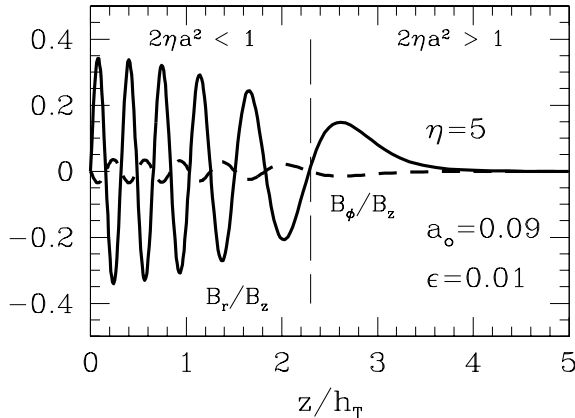


Figure 2. Structure of a weakly magnetized disc with vertical magnetic angular-momentum transport in the limit where no wind develops (channel solution). The dashed line marks the nominal boundary of the MRI-unstable zone discussed in the text.

should not exceed the rate of release of gravitational potential energy.

3 RADIAL TRANSPORT

Numerical simulations indicate that vigorous radial angular momentum transport is sustained by the MRI when the initial (subscript i) Elsasser number $\Lambda_i \equiv v_{Az,i}^2 / \eta_{\text{Ohm}} \Omega_K$ is $\gtrsim 1$ (e.g. Sano & Inutsuka 2001; Sano & Stone 2002a,b), where $v_{Az,i}$ is the (midplane) Alfvén speed based on the initial vertical field $B_{z,i}$ and η_{Ohm} is the Ohmic diffusivity.⁵ Now, for the vertical initial field geometry assumed here, the currents and fields are mutually orthogonal and ambipolar diffusion acts as a field-dependent Ohmic resistivity (e.g. Balbus & Terquem 2001). Under these conditions one can show that $\Lambda_i = \eta_i$, so the minimum-coupling condition in this case is the same for vertical and for radial angular-momentum transport.

What determines which mode of angular momentum transport dominates when the coupling is sufficiently strong ($\eta \gtrsim 1$)? As already noted in Section 1, the MRI is suppressed for sufficiently high values of the field-strength parameter a . A useful clue to the lower limit for MRI stability is provided by the first inequality in equation (1). As discussed in WK93, when this inequality is violated the surface layers of the disc become super-Keplerian, implying outward streaming motion that is unphysical in the context of a pure wind-driving disc model. However, as elaborated on below, an outward motion of part of the disc material is a characteristic of the two-channel MRI mode that underlies MRI-induced turbulence. Further support for this choice of an upper limit on a in the MRI-unstable region is provided by the fact that wind-driving disc solutions that satisfy the constraints expressed by equation (1) are *stable* to the fastest growing linear mode of the MRI, essentially because the minimum wavelength of this mode exceeds the magnetically re-

⁵ Λ is often referred to in the MRI literature as Re_M , the magnetic Reynolds number, but in general $\text{Re}_M \neq \Lambda$.

duced disc scale height (see WK93).⁶ The above limit on a was applied by WK93 at the midplane, since they considered discs in which the entire excess angular momentum of the accretion flow is transported by a wind. As we are now concerned with the possible existence of an alternative mode of transport, we propose to generalize this condition and apply it *locally* (i.e. using $a(z) \propto \rho(z)^{-1/2}$ instead of its midplane value) to differentiate the MRI-unstable section of the disc (where $2\eta a^2 < 1$) from the region where only vertical angular momentum transport takes place ($2\eta a^2 > 1$).

By integrating the disc equations of the model described in Section 2 for the case in which $a < (2\eta)^{-1/2}$ over the bulk of the disc we have verified that such systems do not develop winds. Since our current formulation does not allow for an alternative means of transporting angular momentum through the disc surfaces (such as magnetic braking, “failed” winds that do not cross the relevant critical surfaces, or nonsteady phenomena), the only remaining option is for the angular momentum to be transported magnetically between different heights and then to be carried away radially by bulk flow (with the gas that loses angular momentum moving in and the material that gains angular momentum moving out). Fig. 2 shows a solution of this type. The radial field component oscillates in the region where $2\eta a^2 \lesssim 1$, with B_ϕ exhibiting corresponding oscillations with an opposite sign. The regions where $B_z \partial B_\phi / \partial z < 0$ lose angular momentum to the field and have $v_r < 0$, with the converse behaviour characterizing regions where $B_z \partial B_\phi / \partial z > 0$. We associate this solution with a two-channel MRI mode for the case of a stratified, non-ideal MHD disc.⁷ As was first shown by Goodman & Xu (1994), such modes (which they considered in the unstratified, ideal-MHD case) are exact solutions in both the linear and the nonlinear regimes. Their analysis, however, revealed that these solutions are *unstable* to parasitic modes, and subsequent numerical simulations (carried out in both the ideal and non-ideal regimes) have verified that they rapidly evolve into a turbulent state (e.g. Hawley et al. 1995; Sano et al. 2004, hereafter S04).

To account for the turbulent angular momentum transport that we expect to develop in disc regions where $\eta \gtrsim 1$ and $2a^2\eta \lesssim 1$, we adopt the results of numerical simulations, which have found that the main contribution to the $r\phi$ component of the stress tensor is provided by the turbulent Maxwell stress and that its spatial and temporal average $\ll w_{r\phi} \gg$ can be expressed in terms of the similarly averaged magnetic pressure by

$$\ll w_{r\phi} \gg \approx 0.5 \frac{\ll B^2 \gg}{8\pi} \quad (2)$$

(e.g. Hawley et al. 1995; S04). Using the characteristic ratios $\ll B_\phi^2 \gg / \ll B_z^2 \gg \approx 24$ and $\ll B_r^2 \gg / \ll B_z^2 \gg \approx 3$ for MRI turbulence reported in Table 4 of S04, we substitute $\ll B^2 \gg \approx 28 \ll B_z^2 \gg$ into equation (2) to get

$$\ll w_{r\phi} \gg \approx 14 Y \frac{B_{z,i}^2}{8\pi}, \quad (3)$$

where $Y \equiv \ll B_z^2 \gg / B_{z,i}^2 = Y(\beta)$ is listed in Table 2 of S04

⁶ Note, however, that the formal demonstration of this fact requires using only the third inequality in equation (1).

⁷ Similar field configurations were obtained by Ogilvie & Livio (2001), who also related them to the channel solution.

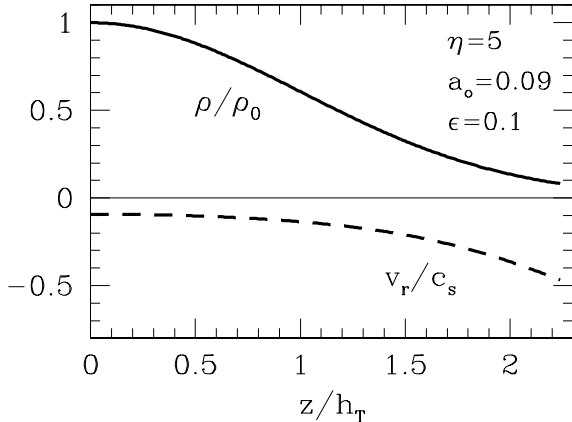


Figure 3. Structure of a weakly magnetized disc with purely radial angular-momentum transport given by the MRI-induced turbulence prescription discussed in the text. The curves terminate at the point where the parameter a satisfies $2\eta a^2 = 1$.

for a range of isothermal, uniform- $B_{z,i}$ models as a function of $\beta_i \equiv 2/a_i^2$, the initial plasma β parameter. As the values of β in our applications are smaller (by up to $\sim 1-2$ orders of magnitude at the midplane) than the ones listed in S04, we resort to extrapolation, which can be justified by the relatively weak dependence of Y on β : we obtain $Y = 2, 7$ and 10 for $\beta = 10, 100$ and 500 , respectively.

Radial angular-momentum transport is incorporated into the disc angular momentum conservation equation by adding (in the relevant disc region) the turbulent stress term, which we do by approximating $(1/r)\partial(r^2 \ll w_{r\phi} \gg)/\partial r \approx \ll w_{r\phi} \gg$. This equation then reads

$$\frac{\rho v_r v_K}{2r} + \rho v_z \frac{dv_\phi}{dz} = -\frac{J_r B_z}{c} - \frac{\ll w_{r\phi} \gg}{r}, \quad (4)$$

where we used $\partial(rv_\phi)/\partial r \approx v_K/2$ and $J_z \approx 0$. We assume that the small-scale (turbulent) magnetic field components only contribute to the radial angular-momentum transport. We interpret all the other magnetic-field (and velocity) terms that appear in the disc structure equations as corresponding to the *mean* values of the respective quantities. In a similar vein, we interpret the first term on the r.h.s. of equation (4) as representing the vertical angular-momentum transport induced by the mean field. This representation is akin to that of previous models that incorporated radial angular-momentum transport into discs threaded by an open magnetic field (see Section 1). The underlying assumptions of this approach – that the relationships obtained from local shear-box simulations remain applicable in a stratified disc, that $\ll B_r B_z \gg$ averages out to zero and that $\ll (B_r^2 + B_\phi^2) \gg$ does not have a significant z dependence – will, however, need to be verified by means of global numerical simulations. According to the above formulation, vertical angular-momentum transport associated with a large-scale, ordered field occurs throughout the disc (with the angular momentum deposited into the mean field eventually transferred back to matter in the wind region above the disc), whereas radial transport effected by MRI-induced turbulence is confined to the layer where the conditions $1 \lesssim \eta \lesssim (2a^2)^{-1}$ are satisfied.

Fig. 3 shows a weak-field disc solution, obtained by implementing the above prescription for the same values of η

and a_0 as in the channel solution presented in Fig. 2. In this case the angular momentum transport is purely radial throughout the disc. The azimuthal field component at the top of the disc does not generally vanish in weak field disc configurations of these type, implying a net vertical torque ($\propto B_z B_{\phi,b}$) on the disc. However, in the current formulation such a torque can only be included if the wind launching condition is satisfied. Since this is not the case here, we chose to eliminate all the magnetic terms from the derived solution for self consistency. The resulting error is, however, small since the mean-field contribution to the disc dynamics (in particular, to angular momentum transport and to vertical squeezing) is rather minor in this instance. The lack of strong magnetic squeezing is reflected in the more gradual decline of the density with height in this solution as compared with the pure wind-driving disc model presented in Fig. 1.

4 COMBINED TRANSPORT

We now consider the case of a disc with moderate coupling ($\eta \sim 1$) and field strength ($a_0 < (2\eta)^{-1/2}$ but $a \sim 1$ at the surface), so both radial angular-momentum transport by a turbulent magnetic field (between the midplane and the height z_t where $2\eta a^2 \approx 1$) and vertical transport by a large-scale field (between $z = 0$ and the top of the disc at z_b) take place at the same radial location. Solutions of this type occupy a limited region of parameter space, corresponding to a large enough a_0 for a wind to be launched from the disc surfaces and a sufficiently small η_0 to render $2\eta_0 a_0^2 < 1$ (but $\eta_0 \gtrsim 1$ so as not to suppress the growth of MRI-unstable modes). We have found that if η is assumed to be both > 1 and constant with height (as was done in the previous Sections), the vertical extent Δz_{MRI} over which radial transport operates is very narrow. The value of Δz_{MRI} is limited by the fact that a_0 has a lower limit below which the wind-driving surface layers of the disc become sub-Keplerian (corresponding to an effective violation of the first inequality in equation 1 in these regions). To circumvent this limitation, we have allowed η to fall slightly below 1 (with the expectation that it is still large enough to sustain MRI turbulence; see Sano & Stone 2002a,b) and to decrease with height. The adopted profile is motivated by the inferred behaviour of $\eta(z)$ in the ambipolar diffusion-dominated upper layers of realistic protostellar discs at $r \sim 1-10$ AU, where the ion density is most strongly affected by the decrease of the neutral gas density with height (see footnote 3).

Fig. 4 shows illustrative solutions obtained under these assumptions. The solid lines depict the structure of the disc when only vertical angular-momentum transport is included (cf. Fig. 1). The dashed lines indicate how the above solution is modified when radial transport is incorporated using the prescription discussed in Section 3 and keeping the value of a_0 fixed. Key properties of the two solutions are compared in Table 1, assuming that c_s and ρ_0 also remain unchanged. The mass accretion rate per disc circumference is evaluated from $\dot{M}_{\text{in}}/2\pi r_0 = -2 \int_0^{z_b} \rho v_r dz$; the listed value ($\dot{\mathcal{M}}_{\text{in}}$) is this quantity normalized by $(\rho_0 c_s h_T)$. The vertical and radial torques (per unit area) on the disc are normalized by $r_0 B_0^2/4\pi$ and are given by $T_z = \kappa\lambda$ and $T_r = (4\pi \ll w_{r\phi} \gg / B_0^2)(\Delta z_{\text{MRI}}/r_0)$, respectively (with

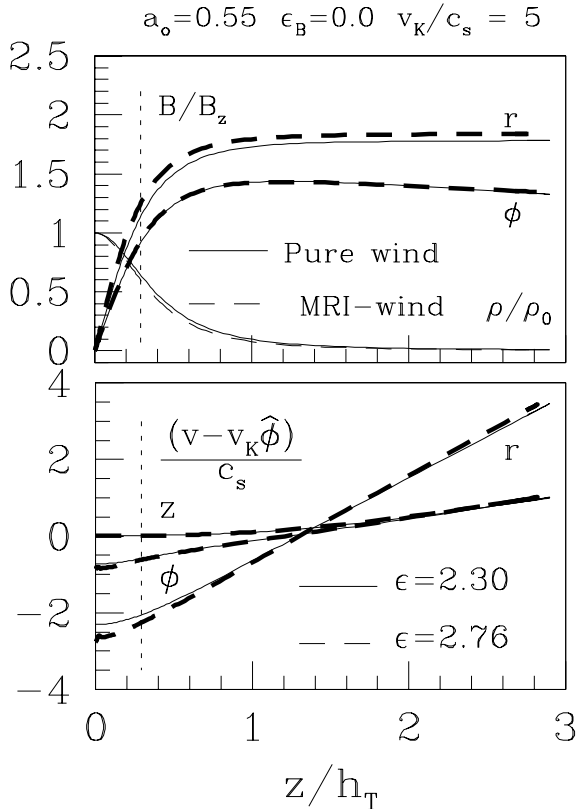


Figure 4. Wind-driving disc with a moderately strong field ($a_0 = 0.55$) and η decreasing from 0.63 to 0.5 between the midplane and the surface. Density, magnetic field components (top) and velocity components (bottom) are shown for a solution that only incorporates vertical angular-momentum transport (solid lines) and also for a case where radial transport is included (dashed lines) in the region where $2\eta a^2 < 1$ (to the left of the vertical dotted line). The curves terminate at the respective sonic points.

$\Delta z_{\text{MRI}} = z_t$ for the given setup), whereas the azimuthal field component at the disc surface is obtained from $|B_{\phi,b}|/B_z = \kappa(\lambda - 1)$. The heights z_t , z_b , and z_s are listed in units of the scale height h , which is determined for each solution as the value of z where the density drops to ρ_0/\sqrt{e} .

The addition of radial angular-momentum transport results in this case in an increased inflow speed (measured by ϵ) and a higher mass inflow rate (\dot{M}_{in}). The higher $|v_r|$ corresponds to a stronger radial neutral-ion drag (since the ions and field remain pinned at the midplane under the assumption that $\epsilon_B = 0$; see footnote 4), and therefore (by the ion radial force-balance condition; see WK93) to a stronger bending of the magnetic field lines away from the vertical (reflected in the higher value of $B_{r,b}$). This, in turn, increases the level of magnetic squeezing (reflected in the lower value of h), resulting in a stronger density stratification. Although the thickness of the disc remains virtually unchanged (at $z_b = 1.25 h_T$) and the height of the sonic point actually goes down in the combined solution (from $2.90 h_T$ to $2.82 h_T$), the increased stratification (measured by z_b/h and z_s/h , respectively) means that the density at the top of the disc is a lower fraction of the midplane density than in the pure wind solution, leading to a lower wind outflow rate (measured by

Table 1. Comparison of the two solutions shown in Fig. 4.

Disc/outflow properties	Pure wind solution	Wind – MRI solution
a_0	0.55	0.55
ϵ	2.30	2.76
h/h_T	0.31	0.29
z_t/h	—	1.01
z_b/h	3.99	4.35
z_s/h	9.25	9.81
ρ_s/ρ_0	1.0×10^{-2}	8.3×10^{-3}
κ	0.17	0.14
λ	9.60	11.38
$\xi'_p \equiv B_{r,b}/B_z$	1.75	1.81
$ B_{\phi,b} /B_z$	1.44	1.43
T_z	1.63	1.59
T_r	—	0.09
\dot{M}_{in}	1.74	1.84

κ) and a correspondingly lower vertical torque (measured by T_z).

The results shown in Fig. 4 illustrate the possibility that the incorporation of MRI-induced turbulence could increase the overall angular momentum transport in the disc, but *reduce* the amount of angular momentum carried away by the wind. It may be worth noting in this connection that the enhanced squeezing of the disc brought about by the addition of radial transport also reduces the width of the turbulent layer in comparison with the value of z_t that would have been estimated from the pure wind solution (in which a increases less rapidly with z). These considerations suggest that the joint operation of the two angular-momentum transport mechanisms might be self-limiting, in which case it would be unlikely to introduce a dynamical instability. This conclusion could be tested through an explicit stability analysis (e.g. Königl 2004 and references therein) or by means of numerical simulations.

5 CONCLUSION

We have constructed a semi-analytic scheme for modeling magnetized protostellar accretion discs. The model takes into account both vertical angular-momentum transport associated with a large-scale magnetic field that threads the disc and drives a centrifugal wind from its surfaces and radial angular-momentum transport through MRI-induced turbulence. A novel feature of this model is an explicit prescription that identifies the vertical extent of the disc region that is susceptible to sustainable MRI turbulence at any given radius and incorporates a turbulent-stress term (based on published results of numerical simulations and related to the local magnitude of the large-scale field) into the angular-momentum conservation relation for this region. Our general scheme employs a tensor-conductivity formalism and incorporates a realistic vertical ionization structure for the disc. However, in this paper we specialize to the ambipolar diffusion-dominated regime and assume that the ion density is nearly constant with height. This allows us to compare our results with the pure vertical-transport solutions obtained for this case by WK93 and to use the algebraic relations de-

rived in that paper in the analysis of the combined vertical and radial transport.

We have concentrated on the case where the neutral-ion coupling parameter η is $\gtrsim 1$, which allows both the wind-driving and MRI-turbulence mechanisms to operate efficiently. Vertical transport through a wind is expected to dominate when the field-strength parameter a (the ratio of the local Alfvén and sound speeds) is sufficiently high ($\lesssim 1$), whereas radial MRI-induced transport should prevail for $a \ll 1$. We constructed a low- a disc solution exhibiting oscillatory field and velocity profiles and suggested that it evidently represents the steady-state analogue in a diffusive (and stratified) disc of the nonlinear MRI channel mode originally identified by Goodman & Xu (1994). Although the question of the stability of stratified channel solutions in the non-ideal MHD regime has not yet been explicitly addressed, the current evidence (from linear analyses and numerical simulations) suggests that they may well be unstable. On the assumption that, in fact, such flows rapidly become turbulent, we incorporated a turbulent-stress prescription (based on the results of numerical simulations) into the angular momentum conservation equation for this region. We showed that, when implemented, this prescription results in an accretion-disc solution featuring pure inflow. We argued that radial angular-momentum transport terminates when $2\eta a^2$ increases above ~ 1 , and we presented a hybrid solution in which this transition occurs at a height z_t below the disc surface (z_b), with radial transport (restricted to the layer $z \lesssim z_t$) augmenting the vertical transport (which operates for all $z \leq z_b$). We found that the joint operation of these two mechanisms at the same radial location in the disc is apparently self-limiting. In particular, we showed that the incorporation of radial transport, while increasing the total amount of angular momentum removed from the inflowing gas, leads to a reduction in the angular momentum flux carried away by the wind.

Our results strongly indicate that the two angular-momentum transport mechanisms are unlikely to have a significant spatial overlap under realistic circumstances. This is because of the stringent constraints that must be satisfied for this to occur: the parameter a must be small enough ($< (2\eta)^{-1/2}$) near the midplane to allow MRI turbulence to develop over a significant vertical extent, but it cannot be so small that the field is too weak to launch a wind (or else that the surface layers become sub-Keplerian). In practice, these constraints require moderate midplane values of a ($a_0 \gtrsim 0.5$) and rather low (and slowly decreasing with height) values of η ($\eta_0 \lesssim 1$), which are unlikely to be attained over measurable radial extents in real discs. If this result indeed applies generally to protostellar discs in the ambipolar diffusion regime then it is of interest to inquire where each of these mechanisms is likely to dominate in such systems.⁸ As an example, we use the normalizations of a_0 and η_0 given (on a scale of ~ 100 AU) by equations (3.50) and (3.51), respectively, of WK93 and the radial scalings ($B \propto r^{-5/4}$, $\rho \propto r^{-3}$, ion density $\rho_{\text{ion}} \propto r^{1/2}$) correspond-

⁸ It is, however, worth pointing out again in this connection that vertical angular-momentum transport mediated by large-scale fields could take place (e.g. in the form of magnetic braking) even if the conditions for wind launching are not fulfilled.

ing to the asymptotic rotational core-collapse solution of Krasnopol'sky & Königl (2002), which imply that $2\eta_0 a_0^2 \propto r$ drops below 1 at $r \sim 40$ AU (with disc winds dominating the angular momentum transport at larger radii and MRI-induced turbulence turning on closer in).

The above example should, of course, be taken only as an illustration, since the radial parameter profiles in actual discs may be quite different. Furthermore, as the density and column density in the disc increase with decreasing radius, the Hall conductivity regime, and eventually also the Ohmic regime, will be encountered (e.g. Balbus & Terquem 2001), with different regimes expected to dominate at different heights at any given radial location (Wardle 2004). We are currently in the process of applying our general scheme to the investigation of the various conductivity regimes in realistic protostellar disc models. The results will be reported in future publications.

ACKNOWLEDGMENTS

We thank the referee for helpful comments. This research was supported in part by a NASA Theoretical Astrophysics Program grant NNG04G178G and by the Australian Research Council.

REFERENCES

Balbus S. A., Hawley J. F., 1998, *Rev. Mod. Phys.*, 70, 1
 Balbus S. A., Terquem C., 2001, *ApJ*, 552, 235
 Blandford R. D., Payne D. G., 1982, *MNRAS*, 199, 883 (BP82)
 Casse F., Ferreira J., 2000, *A&A*, 353, 1115
 Casse F., Keppens R., 2002, *ApJ*, 581, 988
 Glassgold A. E., Feigelson E. D., Montmerle T., Wolk S., 2005,
 in Krot A., Scott E. R. D., Reipurth B., eds, *Chondrites and the Protoplanetary Disk*. ASP Conf. Ser. Vol. 341, p. 165
 Goodman J., Xu G., 1994, *ApJ*, 432, 213
 Hartigan P., Edwards S., Ghandour L., 1995, *ApJ*, 452, 736
 Hawley J. F., Gammie C. F., Balbus S. A., 1995, *ApJ*, 440, 742
 Königl A., 1989, *ApJ*, 342, 208
 Königl A., 1997, in Wickramasinghe, D. T., Bicknell, G. V., Ferriero, L., eds, *Proc. IAU Colloq. 163, Accretion Phenomena and Related Outflows*. ASP Conf. Ser. Vol. 121, p. 551
 Königl A., 2004, *ApJ*, 617, 1267
 Königl A., Pudritz R. E., 2000, in Mannings, V. G., Boss, A. P., Russell, S. eds, *Protostars & Planets IV*. Univ. Arizona Press, Tucson, p. 759
 Krasnopol'sky R., Königl A., 2002, *ApJ*, 580, 987
 Kuwabara T., Shibata K., Kudoh T., & Matsumoto R., 2005,
 ApJ, 621, 921
 Li Z.-Y. 1995, *ApJ*, 444, 848
 Li Z.-Y. 1996, *ApJ*, 465, 855
 Lovelace R. V. E., Romanova M. M., & Newman W. I., 1994,
 ApJ, 437, 136
 Miller K. A., Stone J. M., 2000, *ApJ*, 534, 398
 Ogilvie G. I., Livio M., 2001, *ApJ*, 553, 158
 Pesenti N., Dougados, C., Cabrit, S., Ferreira, J., Casse, F., Garcia, P., O'Brien, D., 2004, *A&A*, 416, L9
 Ray T., dougados C., Bacciotti F., Eisloffel J., Chrysostomou A., 2006, in Reipurth B., Jewitt D., Keil K., eds, *Protostars & Planets V*. Univ. Arizona Press, Tucson, in press (astro-ph/0606697)
 Salmeron R., Wardle M., 2003, *MNRAS*, 345, 992
 Salmeron R., Wardle M., 2005, *MNRAS*, 361, 45
 Sano T., Inutsuka S., 2001, *ApJ*, 561, L179

Sano T., Stone J. M., 2002a, ApJ, 570, 314
Sano T., Stone J. M., 2002b, ApJ, 577, 534
Sano T., Inutsuka S., Turner N., Stone J. M., 2004, ApJ, 605, 321
(S04)
Semenov D., Wiebe D., Henning Th., 2004, A&A, 417, 93
Soker N., Regev O., 2003, A&A, 406, 603
Wardle M., 1999, MNRAS, 307, 849
Wardle M., 2004, Ap&SS, 292, 317
Wardle, M., Königl, A. 1993, ApJ, 410, 218 (WK93)

This paper has been typeset from a \TeX / \LaTeX file prepared
by the author.